ENN Encyclopedia of Nanoscience and Nanotechnology
www.aspbs.com/enn

Optical Fibers for Nanodevices

Jenny M. Tam, Sabine Szunerits,[1] David R. Walt

Tufts University, Medford, Massachusetts, USA

CONTENTS

1. INTRODUCTION

Optical fibers offer a unique platform for the fabrication of a variety of nanostructures and nanodevices. Nanotechnology applications incorporating optical fibers have grown during the past twenty years, and modified optical fibers have been increasingly used in the fabrication of nanodevices. For example, optical fibers have been used in microscopy tools, such as near-field scanning optical microscopy (NSOM), to examine the optical properties of nanostructures. Analyzing the optical properties of nanometer-sized structures has become difficult as measurements and resolution have become diffraction limited [1–3], but NSOM has overcome this hurdle. NSOM uses an optical fiber tapered to a nanometer-sized aperture to bypass the diffraction limit of light. Illuminating a NSOM fiber probe and placing it close to the sample surface can make it possible to examine optical characteristics at the nanometer scale. In addition, NSOM has spawned a variety of devices to tackle some of the limitations with current lithographic technologies for data storage.

Optical fibers have also been used as transducers in sensing devices capable of monitoring and detecting a variety of chemical and biological analytes in different environments (e.g., blood, water, food, waste water) [4, 5]. Intracellular processes inside living cells are more complicated to measure, but optical fibers have been tapered to a nanometer-sized apex and inserted into living cells without damaging them in order to measure cellular responses. As a result, these sensors have been able to further elucidate complex intracellular processes.

The nanometer physical aspects of tapered fibers and bundles of tapered fibers have also been used as templates to fabricate a variety of nanostructures. With the direction of light at nanometer-sized tip apices, photopolymerization can be controlled to form nanometer-sized polymer spots [6]. The nanotips have also been immersed in a heated polymer film, indenting the surface and forming nanometer-sized wells. Fiber optic bundles have also been modified to form arrays of nanowells [7] that have been used as templates for nanofabrication. With the immersion of the nanowell array in a polymer solution, arrays of nanocones were produced.

Fundamental characteristics of fibers and fiber bundles will be examined, as well as how they can be modified for nanodevices. Applications incorporating modified fibers, such as nanotips and nanowells, will be described, as well as new approaches to utilize these devices to overcome limitations that face current technologies.

2. OPTICAL FIBERS

2.1. Fundamental Characteristics of Optical Fibers

Optical fibers act as wave guides, efficiently transmitting light from one end of the fiber to the other. Optical fibers can be made out of glass or plastic, resulting in a strong, flexible, and durable component for a variety of applications. An optical fiber is composed of a core, with a refractive index n_1, surrounded by a cladding with a *lower* refractive index n_2 (Fig. 1). The refractive index mismatch results in total internal reflection at the core-clad interface, effectively acting like a mirror and confining the transmission of light to the fiber core with minimal attenuation. Several principles govern the light transmission through an optical fiber and are significant in their function in nanodevices.

[1]Permanent address: CEA Grenoble, UMR SPrAM 5819, 17, avenue des Martyrs, 38054 Grenoble Cedex, France.

ISBN: 1-58883-064-0/$35.00

Encyclopedia of Nanoscience and Nanotechnology
Edited by H. S. Nalwa
Volume 8: Pages (167–177)

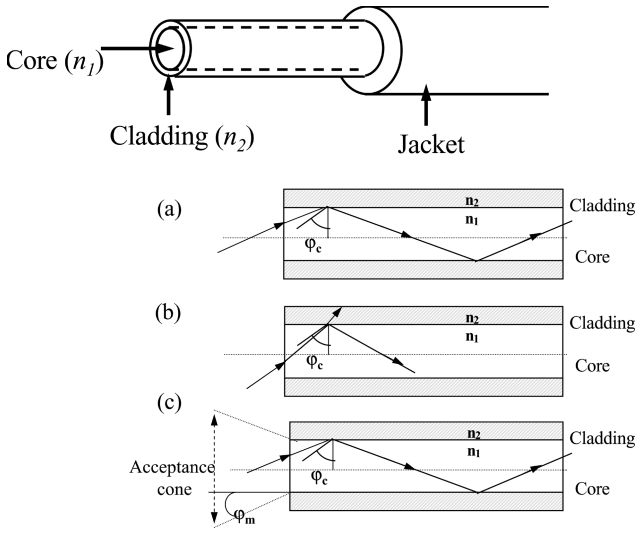

Figure 1. Schematic diagram of an optical fiber with the core and clad structure. Propagation of light through an optical fiber occurs through total internal reflection. Total internal reflection occurs at the interface between the core (n_1) and the clad (n_2), where $n_1 > n_2$. (a) Total internal reflection occurs when the light angle is greater than the critical angle φ_c. (b) Light is partially reflected and partially refracted if the light angle is less than the critical angle φ_c. (c) Total internal reflection will occur only if the entering light angle is within the acceptance cone φ_m of the fiber.

2.1.1. The Critical Angle

The guiding principle for light in an optical wave guide is total internal reflection (Fig. 1). According to Snell's law of refraction

$$n_1 \times \sin \Theta_1 = n_2 \times \sin \Theta_2 \tag{1}$$

For a step-index fiber, where $n_1 > n_2$, total internal reflection occurs when the incident angle Θ_1 meets the criterion $90° > \Theta_1 > \Theta_c$, where Θ_c is given by

$$\Theta_c = \sin^{-1}(n_2/n_1) \tag{2}$$

The critical angle Θ_c depends on the indices of refraction between the core and the cladding. Provided that total internal reflection occurs at the core-clad interface, a ray of light propagates down the core as shown in Figure 1.

2.1.2. Acceptance Cone

High transmission efficiencies in optical fibers are achieved if the angle of the light entering the fiber is within the acceptance cone as shown in Figure 1c. The acceptance cone depends on the refractive indices of the core, clad, and the surrounding medium (n_o)

$$\sin \Theta_a = \frac{\sqrt{n_1^2 - n_2^2}}{n_o}$$

2.1.3. Numerical Aperture

The efficiency of the light collection of the fiber depends on the width of the acceptance cone and can be described in terms of its numerical aperture (NA)

$$\mathrm{NA} = n_o \sin \Theta_a$$

A wide acceptance cone can gather light more efficiently, symbolized by a high NA.

2.2. Types of Optical Fibers

Optical fibers are made from a variety of materials, but the most common material is silica. Pure silica has a refractive index of approximately 1.45, and doping it with various impurities will alter this value. For example, impurities that raise the refractive index include titania (TiO_2), alumina (Al_2O_3), and germania (GeO_2), whereas boria (B_2O_3) and fluorine (F_2) will lower it [8]. Fibers with silica cores surrounded by plastic cladding are also available, as are all-plastic fibers.

2.3. Optical Fiber Configurations

Optical fibers are produced in many different configurations, sizes, and formats. One type of optical fiber consists of a single core surrounded by a clad material. Fiber optics is mainly used in telecommunications applications, but it has also been incorporated into new applications such as microscopy and sensing. Recently, optical fibers have also been integrated into devices to analyze and create nanostructures. For some fiber-optic nanodevices, optical fibers with diameters ranging from 50 to 500 μm are tapered to a nanometer-sized tip for use in nanotechnology applications such as NSOM.

Fiber optic technology can go one step further—instead of using only one strand of fiber, thousands to tens of thousands of optical fibers can be bundled together and used for imaging applications. Single optical fibers cannot transmit images because the light signal mixes as it is carried from one end of the fiber to the other. Fiber optic bundles, on the other hand, are composed of thousands of individual fibers melted and drawn together coherently (Fig. 2), such that an

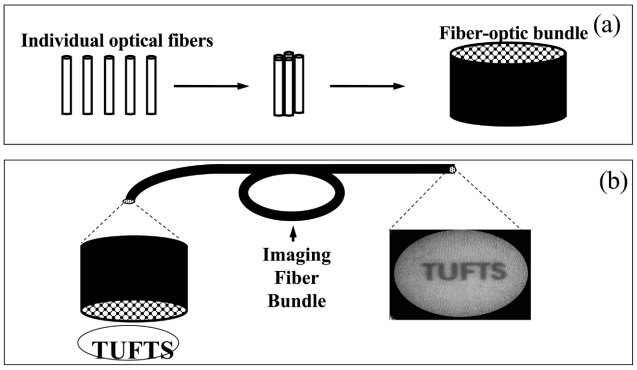

Figure 2. (a) Fiber-optic bundles are composed of thousands to tens of thousands of individual fibers that are coherently fused together. (b) Fiber bundles can be used for imaging purposes. Reprinted with permission from [7], P. Pantano and D. R. Walt, *Chem. Mater.* 8, 2832 (1996). © 1996, American Chemical Society.

image is carried and maintained throughout the length of the bundle. The spatial resolution of the bundle depends on the diameter of each fiber in the bundle. Fiber bundles have been used in devices such as medical endoscopes to transmit images from inaccessible parts of the body to a detector. Optical fiber bundles have also been incorporated into optical sensors and nanodevices [4, 5]. Similar to single core fibers, the surface of the fiber bundles can be mechanically or chemically modified to produce arrays of nanostructures such as nanotips and nanowells.

3. OPTICAL FIBER MODIFICATIONS FOR NANOSCALE APPLICATIONS

3.1. Optical Fibers as Probes in Near-Field Scanning Optical Microscopy

Conventional, far-field optical techniques have limited spatial resolution [9–11]. The typical rules of interference and diffraction are defined by the Abbe diffraction limit, in which the optical resolution is approximately $\lambda/2(\mathrm{NA})$, where λ is the wavelength and NA is the numerical aperture [9]. The rapid development of nanotechnology demands better spatial resolution and has led to the development of alternative microscopy techniques such as near-field optics (NFO) and NSOM. NSOM offers enhanced spatial resolution, bypassing the Abbe diffraction limit by using a small, subwavelength-sized light source that effectively focuses photons through an aperture that may be as small as $\lambda/50$ [9].

NSOM is a scanning technique that developed from principles derived from two other related scanning techniques, scanning tunneling microscopy (STM) and atomic force microscopy (AFM) [12–14]. In 1982, G. Binning and H. Rohrer at the IBM Research Center in Zürich showed that topographic pictures of surfaces on an atomic scale could be obtained by a method they called STM or scanning tunneling microscopy [12]. STM consists of two electrodes, the tip and the sample, and measures the tunneling current between the tip and surface. STM obtains information about both the topographical and electronic surface structure. STM led to the development of other types of microscopy, particularly AFM.

An atomic force microscope creates a topographical image of a surface through physical interactions between a nanometer-sized probe and the sample surface [13, 14]. The probe consists of a sharp tip attached to a cantilever, and an image is created based on the deflection of the tip as it rasters over the sample surface. As a result, each point in the image directly corresponds to the surface structure.

Unlike STM or AFM, NFO images sample through the interaction of light with the surface through simple refraction/reflection contrast or absorption and fluorescence. Introduced by U. During in 1986 [15], NSOM illuminates a specimen through a subwavelength-sized aperture, typically a tapered fiber probe, while keeping the specimen close to the probe, typically 100 Å to tens of nanometers from the fiber. NSOM picks up information contained in the optical field just above the surface of the illuminated sample called the near-field region, where the sample and the probe light closely interact [3]. Radiation emitted from the nanometer-sized probe is highly collimated in the near-field regime, decaying exponentially as photons move away from the surface, as shown in Figure 3. In NSOM, the spatial resolution of a sample is no longer limited by the diffraction limit of light—it is independent of the wavelength of light used and depends only on the size of the aperture. As a result, the quality of NSOM measurements is fully dependent on optical tip parameters, and the resolution is directly related to the size of the probe aperture, which is typically 50–200 nm [16]. Betzig and Chichester have reported the development of one such probe that has an optimum spatial resolution of 12 nm [17]. A NSOM can also supply additional physical information about a sample such as spectroscopic properties, optical thickness, topography, lateral structure, transparency, as well as its chemical behavior. NSOM has been mainly used for analytical applications, but several new NSOM-based applications have been proposed recently for nanotechnology; these are described in Section 4.

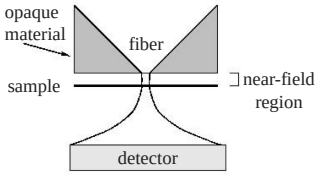

Figure 3. Schematic of near-field optics.

The formation of nanometer-sized fiber probes for microscopy applications, such as NSOM, progressed rapidly during the 1980s and 1990s. In these applications, the formation and characterization of the tips are crucial to instrument performance and image interpretation [18]. Several methods have been used to scale micrometer-size optical fibers for nanotechnology applications.

3.1.1. Mechanical Pulling

One of the preferred methods for fabricating nanometer-sized probes is the mechanical pulling of heated fibers, with either a micropipette puller or a CO_2 laser [19–23]. In a micropipette puller, a small area of the fiber is situated in the center of a heating coil and then the tip of the fiber is pulled until it separates, leaving a long tip [23]. An apparatus used by Tan and co-workers [6] consists of a modified micropipette puller and a 25-W CO_2 infrared laser. The CO_2 laser replaces the heating coil. The laser beam is reflected off a mirror and directed to heat the optical fiber. Similar to the micropipette puller, the fiber is heated and then pulled until the fiber separates into two fibers, each with a long tip. To create nanometer-sized apertures, metal is coated along the length of the tapered fiber. To avoid metallizing and blocking the tip, the tip surface must be positioned essentially orthogonal to the pulled fiber wall [24]. The deposition angle also has to be carefully adapted to the tip geometry.

Mechanical pulling is fast compared with chemical etching (*vide infra*) and is quite controllable, since there is precise control over the heating and pulling parameters. Although transmission is low through pulled fibers, they have well-defined apertures, with diameters as small as 50 nm.

3.1.2. Chemical Etching

Chemical etching produces shorter tapers with larger cone angles, resulting in higher transmission efficiency (shown in Fig. 4) [18, 25–42]. Furthermore, chemical etching offers a simple and inexpensive fabrication method, especially compared with mechanical pulling. Depending on the composition of the glass, different acidic solutions are used. Silica fibers are chemically etched in a one-step procedure with a solution of hydrofluoric acid (HF) and ammonium fluoride (NH_4F) buffer. The etch rate depends on the dopant concentration in the fiber and the concentration of the acid solution. Single core optical fibers and fiber bundles can be etched to form either nanotips or nanowells. For example, in the fiber bundles used by Pantano and Walt [7, 43], the pure SiO_2 of the fiber cladding etches at a different rate than the GeO_2-doped SiO_2 of the core, and depending on the dopant concentration of the core and cladding, either nanotips or nanowells can be formed. Figures 5 and 6 show images of the nanotips and nanowells that can be fabricated. The chemical reaction of SiO_2 and GeO_2 with HF acid can be summarized by reactions (1)–(3) [44].

$$SiO_2 + 6HF \rightarrow H_2SiF_6 + 2H_2O \quad (1a)$$

$$GeO_2 + 6HF \rightarrow H_2GeF_6 + 2H_2O \quad (1b)$$

The fluorosilicic acid (H_2SiF_6) and the hexafluorogermanic acid (H_2GeF_6) are produced directly as outlined by reactions (1a) and (1b) but also can arise from

$$SiO_2 + 4HF \rightarrow SiF_4 + 2H_2O \quad (2a)$$

$$3SiF_4 + 2H_2O \rightarrow 2H_2SiF_6 + SiO_2(aq) \quad (2a)$$

$$GeO_2 + 4HF \rightarrow GeF_4 + 2H_2O \quad (2b)$$

$$3GeF_4 + 2H_2O \rightarrow 2H_2GeF_6 + GeO_2(aq) \quad (2b)$$

If an ammonium fluoride-buffered etching solution is used, there is a further possible dissolution step that arises from the involvement of ammonia ionized from the solution (reaction (3)).

$$H_2SiF_6 + 2NH_3 \rightarrow (NH_4)_2SiF_6 \quad (3a)$$

$$H_2GeF_6 + 2NH_3 \rightarrow (NH_4)_2GeF_6 \quad (3b)$$

The difference in solubility of the resultant $(NH_4)_2SiF_6$ and $(NH_4)_2GeF_6$ leads to different etching rates between the core and cladding. Therefore, the tip cone angle is a function of the concentration of etchant solution and the GeO_2 dopant level of the fiber core. Temperature can also influence the tip cone angle [18].

Etching parameters such as solvent type, acid concentration, etching time, and temperature are crucial for optical and geometrical characteristics (e.g., cone angle, aperture diameter, well size); Table 1 lists some of the conditions used in the literature. Recently, it was shown that a multiple-step etching process followed by application of an organic protecting layer improved optical characteristics of the fibers [37]. Stöckle developed a specific chemical etching method called tube etching. It involves etching fiber tips surrounded with an organic cladding where the acid first etches away the tip of the fiber without destroying the cladding [45]. The polymer cladding is thus acting as a wall, creating microcurrents in the acid, which, coupled with capillary action, cause the fiber to be etched into the shape of a cone with a large, smooth taper.

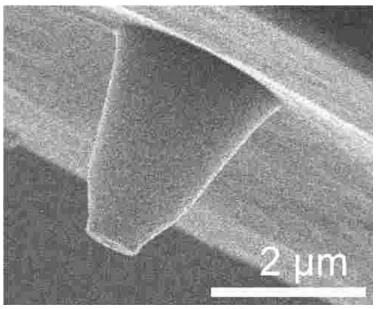

Figure 4. Etched fiber optic for use as a NSOM probe. Reprinted with permission from JASCO Inc.

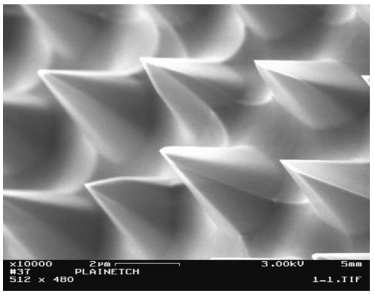

Figure 5. Scanning electron micrograph of an array of nanotips formed by chemical etching of a fiber-optic bundle.

3.1.3. Fracturing

Fischer and co-workers [46, 47] fabricated tetrahedral tips for NSOM, using modified ultramicrotome glass blades. A rectangular slab of glass was cleaved twice at an angle. A tetrahedral tip consists of a pyramidal glass fragment, which is then coated with a gold film. The tetrahedral tip is mounted on the oblique end face of a glass support by an index matching glue. A beam of light incident at an angle of 45° can irradiate the tip.

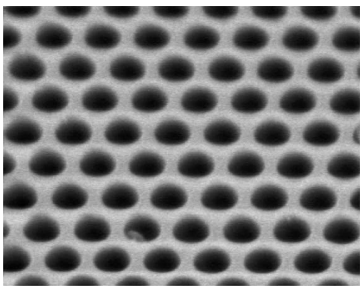

Figure 6. Scanning electron micrograph of a nanowell array formed by chemical etching of a fiber-optic bundle. The doping concentration in the core and clad material determines whether nanotips or nanowells will be formed.

Table 1. Etching conditions and the optical fiber apertures obtained.

	Mode	Fiber	Time temp.	Solution	Characteristics	Comments	Ref.
1	SM	Silica glass fiber FS-SN-3224, 3 M C 4 μm/ G 125 μm	21 °C 140 min	HF (40%)	CA 50°–80°	Bevelling	[93, 94]
2	SM	Silica glass fiber Newport F-SF		HF (48%), NH_4F (40%) water ratio = 1:x:1 x = 1.5, 7	CA 8°–90°	Organic solvent as protection	[37]
3	SM	Silica glass fiber FS-SN-3224, 3 M C 3 μm	10–50 °C, 90 min	HF (21, 28, 34, 40%)	CA 18°–35°	p-Xylene as protection	[45]
		Silica glass fiber 40-692.11, Cabloptioc, C 3 μm					
		Silica glass fiber 91-9116.136, Alcatel C 3 μm					
	MM	HCG-M0100T-14, Laser Components C 100 μm					
	MM	HCG-M0200T-14, Laser Components C 200 μm core					
4	SM	Bent SNOM tip	132 min	HF (48%), acetic acid ratio = 7:1	CA 40° 50-nm tip radii	Two-stage hexadecane	[39]
5	SM	GeO_2-doped core	—	—	CA 150° 25 nm	Three-stage etching	[28]
7	IF	Sumitomo Electric Industries, IGN-035/06	RT 16 h	HF (50%), NH_4F (40%) water ratio = 1:5:1	Tip diameter 300 nm		[43]
8	MM	Silica glass fiber Corning 6 62-125-900 ST	24–50 °C 1–20 h	HF (50%), NH_4F (40%) water ratio = 1:x:1 x = 2, 4, 6	CA 36°–140°		[18, 95]
9	IF	Sumitomo Electric Industries, IGN-035/06	RT 7.5 h	HF (49%), NH_4F (40%) water glacial acetic acid ratio = 1:6:1:1	CA 25° Radius of tip 15–50 nm		[88]
10	SM	GeO_2-doped silica fibers (3.6–23 mol%)	22 °C 180 min	HF (50%), NH_4F (40%) water ratio = 1:x:1 x = 4, 5, 6, 7	CA 20° Tip diameter 10 nm		[36]

Note: SM, single mode; MM, multiple mode; IF, imaging fiber; C, cone; G, cladding; CA, cone angle.

4. FIBER OPTIC-BASED NANODEVICES

4.1. NSOM-Based Applications in Nanotechnology

4.1.1. NSOM-Based Optical Storage

In addition to its use in analytical applications as well as in the detection of nanostructures ([48–50] and references therein), NSOM is also used for data storage applications. Data are written and read off of optical storage devices by using a focused laser beam on a storage medium [51]. The data density on optical storage disks is determined by the size of the focused laser spot, which is determined by the diffraction limit of light, approximately $\lambda/2$(NA). The diffraction limit can be overcome, however, by NFO techniques, as discussed previously. Smaller spot sizes can increase the areal density over what is currently available on storage devices.

Near-field techniques were used to write and read data [52–60] domains as small as 60 nm in thin-film magneto-optic materials [61]. As shown in Figure 7, a dichroic mirror splits a beam from an Ar laser into two distinct wavelengths. One beam is used for reading, and another is used for writing. The beam used for reading is attenuated with a neutral-density filter, while the writing beam is controlled with an acousto-optic modulator. The beams are then recombined and coupled into an optical fiber NSOM probe. Half-wave ($\lambda/2$) and quarter-wave ($\lambda/4$) plates, positioned before the fiber coupler, adjust the polarization of the laser light to an almost purely linear state. The Faraday effect rotates

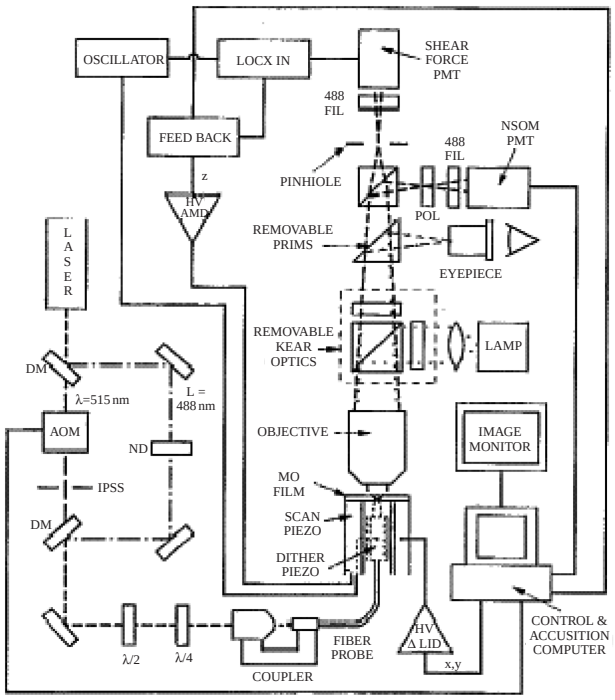

Figure 7. Schematic of system used for near-field magneto-optic imaging and recording. Reprinted with permission from [61], E. Betzig et al. *Appl. Phys. Lett.* 61, 142 (1992). © 1992, American Institute of Physics.

the polarization of the light slightly as it passes through the magneto-optical film. The direction of the rotation is determined by the orientation of the magnetization immediately under the probe. A conventional optical microscope then collects the light, and the image is viewed with a polarizer/photomultiplier tube combination.

The acousto-optical modulated laser beam writes data on the magneto-optical storage medium by heating the data region under the probe near the Curie temperature [61], magnetizing the domain in a direction opposite that of the surrounding medium. After writing, the data are then read with the lower power read beam. An example of written data is shown in Figure 8.

The data domains are approximately 100 nm in diameter with a 200-nm center-to-center spacing. The polarization of the aperture is rotated by approximately $+1°$ and $-1°$ (Fig. 9a and b, respectively). The pattern on the storage medium is imaged as it appears, composed of alternating contrast regions. Although high laser power may be required, the entire reading and writing process is straightforward.

4.1.2. NSOM Optical Lithography

The smallest structures that can be achieved with conventional optical lithography are determined by the Abbe diffraction limit. Although shorter wavelengths (UV, X-rays) and particle beams have brought the feature sizes down to a few nanometers, the setups are costly. NFO lithography was investigated as a method to bypass the limitations faced in conventional optical lithography [62–64].

A near-field lithographic probe was fabricated by drawing an optical fiber while it was heated with a CO_2 laser. The tapered ends were subsequently coated with an approximately

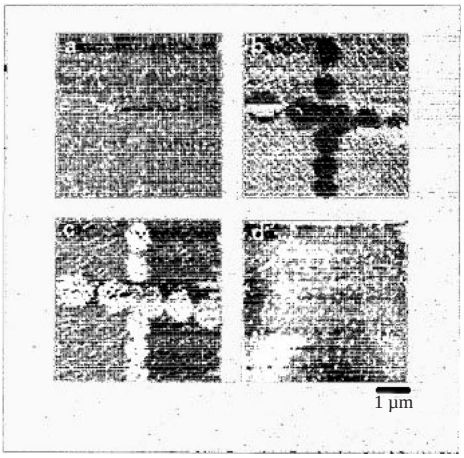

Figure 8. (a–c) Near-field magneto-optic images of conventionally written domains at three different polarization states. (d) Topographical image of the same region obtained with shear force microscopy. Reprinted with permission from [61], E. Betzig et al., *Appl. Phys. Lett.* 61, 142 (1992). © 1992, American Institute of Physics.

100-nm layer of aluminum. Typical aperture sizes of about 50 nm were achieved.

As shown in Figure 10, a photoresist sample was mounted on a piezoelectric motor and was placed in proximity to the near-field probe, approximately 10 nm away. An Ar laser was coupled into the optical fiber that was connected to a fiber coupler. An acousto-optical modulator was placed in the laser beam to control the exposure of the laser light to the photoresist. Lines about 80 nm wide and 10 nm deep were written on the surface upon exposure to laser light emitted from the probe. The surface structures were analyzed with an AFM, as shown in Figure 11.

4.1.3. Near-Field Optical Array

Single probes in conventional NSOMs are limited in that they can only examine one particular region at a time [6, 65]. Pantano and Walt [7, 43] fabricated a NFO array

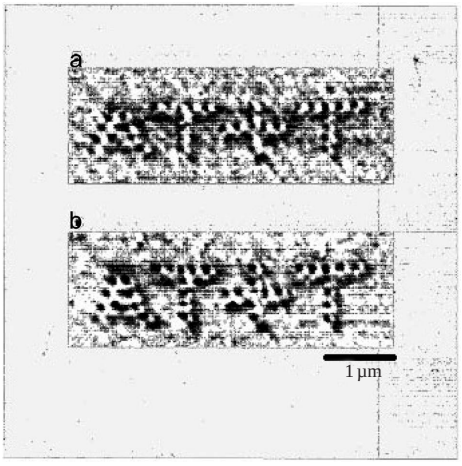

Figure 9. Written domains with ~100-nm diameters formed and imaged with near-field techniques. Two different polarization states are shown in (a) and (b). Reprinted with permission from [61], E. Betzig et al. *Appl. Phys. Lett.* 61, 142 (1992). © 1992, American Institute of Physics.

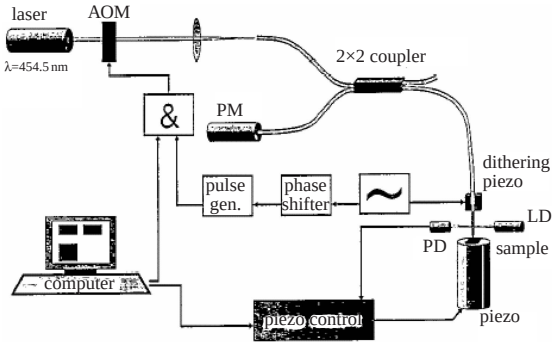

Figure 10. Schematic view of experimental setup used for NSOM lithography. Reprinted with permission from [96], G. Krausch et al., *Thin Solid Films* 264, 264 (1995). © 1995, Elsevier Science.

that can overcome this limitation. A 300-μm-diameter imaging fiber bundle, comprising approximately 6000 coherently fused optical fibers, was chemically etched in a buffered HF solution for 16 h, yielding an array of near-field tips (shown in Fig. 12).

To prevent light leakage from the sidewalls of each tip in the array, a gold layer coated the entire array. The entire array was crudely ground on a spinning mirror to create nanoapertures on each tip. Metal-coated tips with apertures as small as 300 nm were fabricated, and the height differences between near-neighbor tips were as small as approximately 20 nm, as shown in Figure 13. The optical properties of the array were also investigated by directing light through the proximal end of the fiber and imaging a small portion of the distal face through a microscope objective.

The major advantage of a near-field array is that it can scan a larger area of a sample. For example, in an equivalent period of time, an array of several thousand 100-nm-diameter near-field tips on the distal face of a 300-mm-diameter fiber bundle could scan over an area approximately three orders of magnitude larger than that of a single 100-nm-sized tip. In addition, commercial imaging fibers are available with up to 100,000 individually clad optical fibers such that very large regions can be imaged with subwavelength resolution.

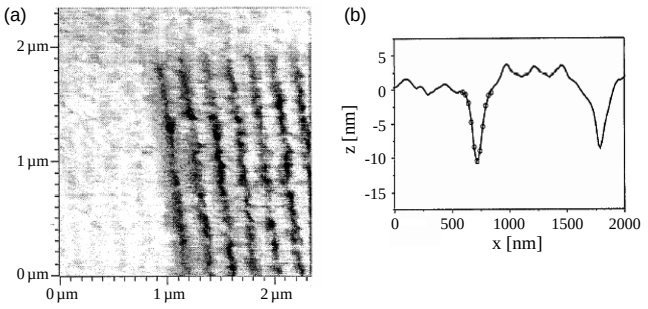

Figure 11. AFM images of lines created by near-field scanning lithography. (a) Top view of a set of parallel lines created by a single path exposure through the tapered tip of an optical fiber. (b) A cross-sectional view of two written lines. The open circles represent a least-squares fit of a Gaussian profile to the data. Reprinted with permission from [96], G. Krausch et al., *Thin Solid Films* 264, 264 (1995). © 1995, Elsevier Science.

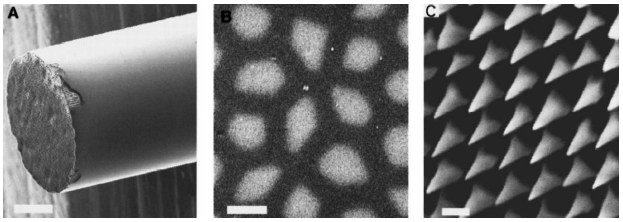

Figure 12. (A) A low-magnification scanning electron micrograph of a chemically etched fiber bundle. The white bar denotes a 50-μm distance. (B) A high-magnification image of the fiber surface *before* it was chemically etched. The white bar denotes a 2.5-μm distance. (C) A high-magnification image of the fiber bundle after it was chemically etched, forming an array of nanotips. The white bar denotes a 2.0-μm distance. Reprinted with permission from [43], P. Pantano and D. R. Walt, *Rev. Sci. Instrum.* 68, 1357 (1997). © 1997, American Institute of Physics.

4.2. Nanosensors

The resolution obtained in near-field microscopy has become useful for single molecule detection [66–69]. Nanoprobes have detected single dye and dye-labeled DNA molecules [48, 70]. The probes had a 100-nm resolution and were able to image labeled DNA molecules. Nanofibers can probe for specific chemicals in highly localized areas, capable of monitoring concentration gradients and spatial homogeneities in cellular environments. Kopelman et al. [6, 71] reported the first nanobiosensor to monitor the environment inside rat embryos. Measurements of Na^+ and Ca^{2+} were also analyzed [72]. These conventional sensors are based on the measurement of fluorescence intensity or on the measurement of luminescence decay time [73].

4.2.1. Nano-Bio-Optrodes

The recent drive in nanotechnology research has led to the development of the nano-bio-optrode, a device that is able to monitor biomolecular concentrations inside a single living cell, elucidating more about the complex intracellular processes that occur [6, 10, 74].

Nano-bio-optrodes are composed of optical fibers a few nanometers in diameter. The optical fiber initially has a diameter of a few micrometers before a modified micropipette puller heats and pulls it to form the bio-optrode.

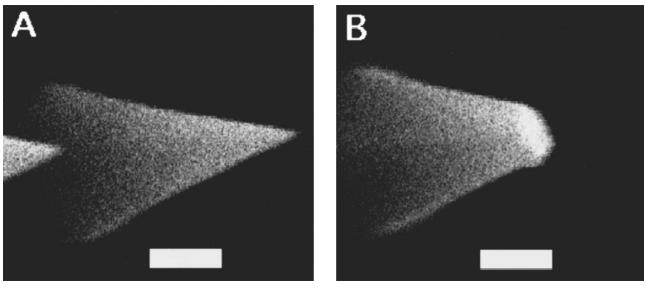

Figure 13. High-magnification scanning electron micrographs of a gold-coated, chemically etched fiber before (A) and after (B) it was ground on a spinning mirror. The white bars denote a 0.5-μm distance. Reprinted with permission from [43], P. Pantano and D. R. Walt, *Rev. Sci. Instrum.* 68, 1357 (1997). © 1997, American Institute of Physics.

The distal tip of the tapered fiber typically has a diameter between 20 and 80 nm. Kopelman and co-workers [65] used this technique to fabricate nano-fiber-optic chemical sensors to monitor the pH inside living cells. A pH-sensitive dye was immobilized on the surface of the fiber tip in a polymer hydrogel to measure the pH changes.

An enzyme-based nano-bio-optrode was also used to measure nitric oxide content [75]. Fluorescently labeled cytochrome c' was immobilized on the tip of the fiber. In the presence of NO, cytochrome c' undergoes a conformational change. Nitric oxide concentration changes were correlated to changes in the energy transfer between cytochrome c' and the fluorescent dye.

Vo-Dinh and co-workers fabricated an antibody-based nano-bio-optrode to detect benzo[a]pyrenetetrol (BPT) [76–78]. The outer walls of the tapered end of a 200-nm to 300-nm fiber were coated with a thin silver, gold, or aluminum layer with the use of a vacuum evaporator as shown in Figure 14. A turning plate/motor device held and rotated the fiber in the deposition chamber. The fiber was held at an angle relative to the metal vapor, and as it rotated, the metal evenly coated the sides of the fiber while leaving the tip uncoated. The metal coating prevents light from leaking from the fiber walls and maximizes the light intensity at the fiber tip. The uncoated tip surface was then silanized to covalently attach anti-BPT antibodies.

Figure 15 shows how the nano-bio-optrode measured BPT concentrations inside a single living cell. The tapered end of the fiber was inserted at an angle inside a living cell and incubated for 5 min to allow the antibodies to bind the antigen (BPT). Laser light was transmitted through the fiber and excited the fluorescent BPT. Bound BPT molecules changed the fluorescence signal. The fiber was then removed from the cell, and the fluorescence signal obtained from the bound BPT was collected through a microscope objective and measured and analyzed with a photomultiplier tube.

Nano-bio-optrodes are advantageous over larger bio-optrodes in that they have higher sensitivities and faster response times. Nano-bio-optrodes could detect BPT concentrations as low as 300 zeptomoles.

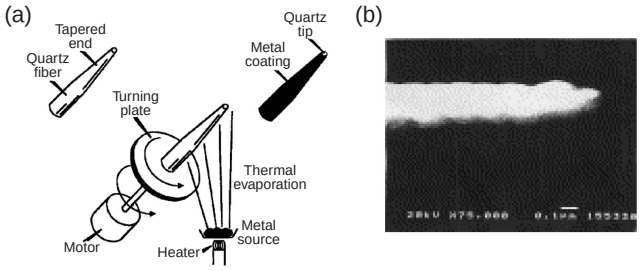

Figure 14. Fabricating nano-bio-optrodes. (a) An optical fiber heated and then tapered to submicron dimensions. Metal is then thermally evaporated on the fiber sidewalls to prevent light leakage. The fiber is mounted on a rotating plate, evaporating an even coating while creating an aperture. Antibodies can be immobilized on the bare distal tip. Reprinted with permission from [77], T. Vo-Dinh et al., *Nat. Biotechnol.* 18, 264 (2000), © 2000, Nature Publishing Group; and [78], T. Vo-Dinh et al., *Sens. Actuators, B* 74, 2 (2001), © 2001, Elsevier Science.

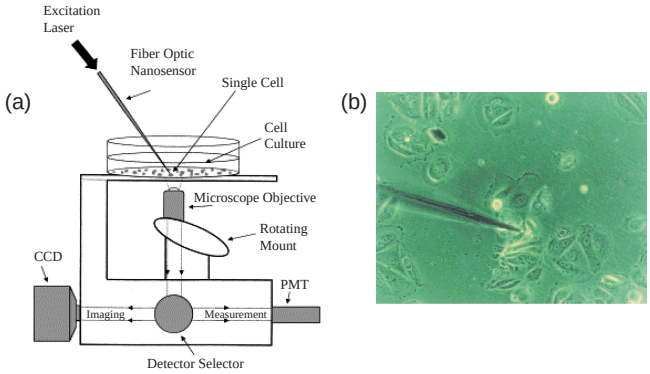

Figure 15. (a) The optical measurement system to monitor living cells. (b) A nano-bio-optrode inside a living cell. Reprinted with permission from [77], T. Vo-Dinh et al., *Nat. Biotechnol.* 18, 264 (2000). © 2000, Nature Publishing Group; and [78], T. Vo-Dinh et al., *Sens. Actuators, B* 74, 2 (2001). © 2001, Elsevier Science.

4.2.2. Fiber Bundle-Based Nanotip pH Sensor

The desire to miniaturize analytical detectors such that data throughput can be increased while small volume samples are used has fueled the rapid development of nanobioanalytical techniques. Another desire in new imaging methodologies involves remote analysis of samples, without having to bring the sample to the microscope stage. A nanotip array, fabricated by chemically etching an imaging fiber bundle, was used to measure oxidative stress in biological cells [22].

Oxidative stress results in an overload of reactive oxygen species, such as hydrogen peroxide, and causes a pH change in cells. Oxidative stress is thought to be an important causative agent in a variety of pathologies such as aging, cardiovascular disease, some carcinogenesis, and possibly in AIDS. Conventional amperometric measurement techniques analyze oxidative stress by inserting the tip of a 5-μm carbon-fiber microelectrode into a biological cell. Analysis indicated that the hydrogen peroxide was generated as a direct result of the microelectrode insertion [79–82]. A nanotip array would improve conventional oxidative stress monitoring techniques because the nanometer dimensions of the tip would be less intrusive to the cell. A nanotip array should also increase measurement throughput by providing sampling through many probes instead of using only one, and the nanotip array's sensing layer can be readily modified to allow investigation of a variety of biologically relevant analytes.

A nanotip array was fabricated by chemically etching a fiber bundle with HF, as discussed in Section 4.1.3, and a chemical sensing layer was deposited across the array such that the nanotip architecture was retained. In addition to its remote sensing abilities and measurement throughput improvements, the small nanotip diameters (ca. 200 nm) of the nanotip array should more closely mimic the size scale of biological entities such as bacteria and viruses in comparison with a conventional 5-μm microelectrode tip.

4.3. Fiber Bundle-Based Photoimprint Lithography

Well-established methods such as electron beam, X-ray, and UV lithographic methods have been used to create nanostructures [83–86] (Sun, 2002 #152, 87). Dam and Pantano [88] created a nanotip array by chemically etching fiber-optic imaging bundles as described in the previous sections. An array of tips was produced as a lithographic template for surface patterning applications. As shown in Figure 16, two methods were used to pattern a polymer surface: photoimprint lithography and imprint lithography.

Both techniques produced arrays of picoliter-volume wells suitable for microanalytical applications. In photoimprint lithography, a patterned surface was created when the nanotip array was brought into contact with a photopolymerizable monomer film, and photoinitiation was directed through the array. With this method, an array of 1-μm wells was produced with a 4-μm center-to-center spacing. In imprint lithography, bringing the nanotip array into contact with a heated polystyrene-covered surface created a patterned surface. With this technique, an array of 0.8-μm-radii wells was produced with 3-μm cone depths and 25° cone angles, as shown in Figure 17.

4.4. Ordered Nanowell Arrays

Lithographic procedures such as microcontact printing [89], high-throughput imprint lithographic methods [90, 91], and nanochannel array glass materials [92] have been used to form ordered, periodic structures on a variety of materials. Arrays of nanowells were fabricated from fiber-optic bundles as another form of templating. Pantano and Walt [7, 43] produced arrays of nanowells with approximately 300-nm diameters, using an embossing template to create patterned polymeric films.

Fiber-optic imaging bundles were polished with a series of lapping films. The fiber bundle was then pulled with a standard micropipette puller and potted in epoxy such that the length of the imaging fiber's distal tip protruded from the polishing apparatus. Adjusting the length of the fiber

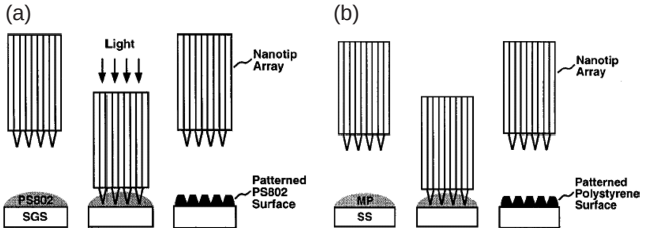

Figure 16. (a) Photoimprint lithography through a nanotip array. A PS802 polymer film is placed on a silicon glass surface. The nanotip array is then brought into contact with the film and glass surface, and light is directed through the fiber bundle, exposing the surface to light. The tip array is then removed, leaving a polymerized, patterned surface. (b) Imprint lithography with a nanotip array. An aluminum surface is coated with melted polystyrene. The nanotip array is then brought into contact with the warm polymer film. The array is then removed, leaving a patterned polystyrene surface. Reprinted with permission from [88], T. H. Dam and P. Pantano, *Rev. Sci. Instrum.* 70, 3982 (1999). © 1999, American Institute of Physics.

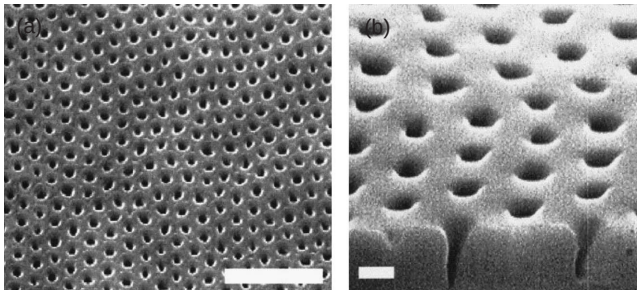

Figure 17. (a) Scanning electron micrograph of a patterned PS802 polymer surface using photoimprint lithography through a nanotip array. The white scale bar denotes a 5-μm distance. (b) A patterned polystyrene surface using imprint lithography through a nanotip array. The white scale bar denotes a 2-μm distance. Reprinted with permission from [88], T. H. Dam and P. Pantano, *Rev. Sci. Instrum.* 70, 3982 (1999). © 1999, American Institute of Physics.

yielded the final, desired diameter of the tapered fiber. The fiber bundle was then chemically etched in a buffered HF solution, yielding an array of nanowells. Scanning electron microscopy and AFM were used to characterize the surface of the modified fiber bundle, as shown in Figure 18. Nanowells with diameters as small as 480 nm with 4.5-μm center-to-center spacings and 300-nm well depths (corresponding to ~2 fL volumes) could be obtained. Such small wells could be used, in principle, as nanoreaction vials for molecule trapping.

The resulting nanowell arrays were used to emboss polymeric films with nanometer-sized structures. The nanowell array was dipped into a siloxane copolymer solution and allowed to cure. The polymer cured upon solvent evaporation, and the dip process was repeated five times. The polymer film was then peeled off of the fiber, resulting in a

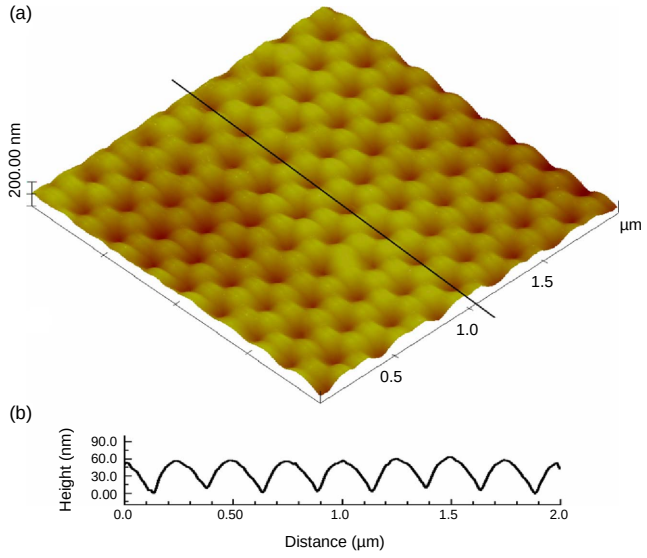

Figure 18. Atomic force micrograph of a modified fiber bundle. The fiber was first mechanically pulled and then was chemically etched to form an array of nanowells. Reprinted with permission from [7], P. Pantano and D. R. Walt, *Chem. Mater.* 8, 2832 (1996). © 1996, American Chemical Society.

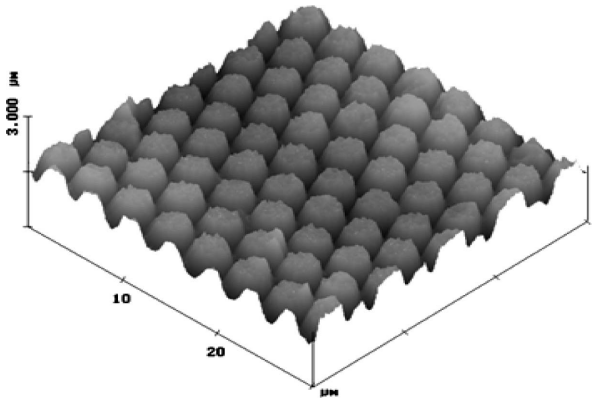

Figure 19. A patterned polymer surface fabricated from an array of nanowells. A polymer layer was deposited on the surface of the nanowell array and removed to form an array of nanocones. Reprinted with permission from [7], P. Pantano and D. R. Walt, *Chem. Mater.* 8, 2832 (1996). © 1996, American Chemical Society.

hexagonally packed array with 600-nm tall cones, as shown in Figure 19.

5. CONCLUSIONS

A variety of techniques have been used to fabricate nanometer-sized optical fiber tips and arrays of nanotips and nanowells from optical fiber bundles. The nanoprobes and arrays of nanoprobes have been successfully applied in NSOM, near-field data storage, and near-field lithography. These systems overcome the diffraction limit, enabling one to study materials science and biomedical phenomena on the nanometer scale. Near-field methods have also been applied to data storage with the potential to create data densities higher than those currently available. NFO lithography can provide a potentially low-cost alternative to conventional lithographic techniques while improving the spatial resolution on substrates. With nanoprobes and arrays of nanoprobes, nanosensors for nitric oxide monitoring and oxidative stress monitoring can be created with higher temporal resolution, greater data throughput, and increased sensitivity. The large variety of nanoprobes will lead to new techniques and applications where progress has been limited by present technologies. In addition, arrays of nanowells have been fabricated for use as nanometer-sized templates for polymer films. As nanotechnology research advances, optical fibers will be further integrated with nanodevices, producing tools that will improve and enhance conventional tools used in scientific research and development.

GLOSSARY

Chemical etching Process of etching by a chemical reaction between a chemically reactive etching species and the material.

Near-field scanning optical microscopy (NSOM) [Also referred to as scanning near-field microscopy (SNOM)]. A scanning probe microscopy technique that analyzes the optical properties of a surface (e.g., fluorescence transmission, reflectance). The specimen is placed less than a wavelength away from the probe, and light is transmitted through a subwavelength-sized aperture as the surface is scanned.

Optical fiber Glass or plastic rod consisting of a core surrounded by a cladding material with a higher refractive index that results in total internal reflection light and confines light to the core. As a result, light is efficiently transmitted with minimal attenuation.

REFERENCES

1. D. W. Pohl, "Advances in Optical and Electron Microscopy." Academic Press, New York, 1991.
2. D. W. Pohl and D. Courjon, "Near Field Optics," NATO ASI Series E. Kluwer, Dordrecht, the Netherlands, 1993.
3. D. Courjon and D. Bainier, *Rep. Prog. Phys.* 57, 1029 (1994).
4. O. S. Wolfbeis, *Anal. Chem.* 72, 81 (2000).
5. O. S. Wolfbeis, *Anal. Chem.* 74, 2663 (2002).
6. W. Tan, Z.-Y. Shi, and R. Kopelman, *Anal. Chem.* 64, 2985 (1992).
7. P. Pantano and D. R. Walt, *Chem. Mater.* 8, 2832 (1996).
8. J. Wilson and J. Hawkes, "Optoelectronics, An Introduction." Prentice Hall, London, 1998.
9. E. Abbe, *Arch. Mikrosk. Anat.* 9, 413 (1873).
10. A. Lewis, M. Issacson, A. Muray, and A. Harootunian, *Ultramicroscopy* 13, 227 (1984).
11. K. Lieberman, S. Harush, A. Lewis, and R. Kopelman, *Science* 247, 59 (1990).
12. G. Binning, H. Rohrer, C. Gerber, and W. Weibel, *Phys. Rev. Lett.* 49, 57 (1982).
13. G. Binning, C. F. Quate, and C. Gerber, *Phys. Rev. Lett.* 56, 930 (1986).
14. M. Y. Reetz, W. Helbig, S. A. l. Quaiser, U. Stimming, N. Breuer, and R. Vogel, *Science* 267, 367 (1990).
15. U. Durig, D. W. Pohl, and F. Rohner, *J. Appl. Phys.* 59, 3318 (1986).
16. S. Seebacher, W. Osten, V. P. Veiko, and N. B. Voznessenski, *Opt. Lasers Eng.* 36, 451 (2001).
17. E. Betzig and R. Chichester, *Science* 262, 1422 (1993).
18. B. A. F. Puygranier and P. Dawson, *Ultramicroscopy* 85, 235 (2000).
19. E. Betzig, J. K. Trautman, T. D. Harris, J. S. Weiner, and R. L. Kostelak, *Science* 251, 1468 (1991).
20. W. P. Ambrose, P. M. Goodwin, J. C. Martin, and R. A. Keller, *Science* 265, 364 (1994).
21. N. Essaidi, Y. Chen, V. Kottler, E. Cambril, C. Mayeux, N. Ronarch, and C. Vieu, *Appl. Opt.* 37, 609 (1998).
22. Y.-H. Liu, T. H. Dam, and P. Pantano, *Anal. Chim. Acta* 419, 215 (2000).
23. G. A. Valaskovic, M. Holton, and G. H. Morrison, *Appl. Opt.* 34, 1215 (1995).
24. W. Tan and R. Kopelman (1996).
25. S. Mononobe, M. Naya, T. Saiki, and M. Ohtsu, *Appl. Opt.* 36, 1496 (1997).
26. S. Mononobe and M. Ohtsu, *J. Lightwave Technol.* 14, 2231 (1996).
27. S. Mononobe and M. Ohtsu, *J. Lightwave Technol.* 15, 1051 (1997).
28. T. Yatsui, M. Kourogi, and M. Ohtsu, *Appl. Phys. Lett.* 73, 2090 (1998).
29. P. Hofmann and R. Slathe, *Ultramicroscopy* 61, 165 (1995).
30. R. U. Maheswari, S. Mononobe, and M. Ohtsu, *J. Lightwave Technol.* 13, 2308 (1995).
31. M. Ohtsu, *J. Lightwave Technol.* 13, 1200 (1995).
32. T. Saiki, S. Mononobe, M. Ohtsu, N. Saito, and J. Kusano, *Appl. Phys. Lett.* 68, 2612 (1996).
33. H.-D. Lee, H.-J. Lee, C.-K. Kim, and C.-H. Han, *Appl. Phys. Lett.* 66, 3272 (1995).
34. S. Ottow, V. Lehmann, and H. Foll, *J. Electrochem. Soc.* 143, 385 (1996).
35. T. Pangaribuan, S. Jiang, and M. Ohtsu, *Electron. Lett.* 29, 1978 (1993).

36. T. Pangaribuan, K. Yamada, S. Jiang, H. Ohsawa, and M. Ohtsu, *Jpn. J. Appl. Phys.* 31, L1302 (1992).
37. Y.-H. Chuang, K.-G. Sun, C.-J. Wang, J. Y. Huang, and C.-L. Pan, *Rev. Sci. Instrum.* 69, 437 (1998).
38. M. Datta, *J. Electrochem. Soc.* 142, 3801 (1995).
39. J. F. Wolf, P. E. Hillner, R. Bilewicz, P. Kolsch, and J. P. Rabe, *Rev. Sci. Instrum.* 70, 2751 (1999).
40. A. Sayah, C. Philipona, P. Lambelet, M. Pfeffer, and F. Marquis-Weible, *Ultramicroscopy* 71, 59 (1998).
41. K. Kobayashi, Y. Nishida, and K. Fujiura, Japanese Patent 09328335, 1997.
42. E. Oesterschulze, O. Rudow, C. Mihalcea, W. Scholz, and S. Werner, *Ultramicroscopy* 71, 85 (1998).
43. P. Pantano and D. R. Walt, *Rev. Sci. Instrum.* 68, 1357 (1997).
44. E. G. Rochow, "Comprehensive Inorganic Chemistry." Pergamon Press, Oxford, 1973.
45. R. Stöckle, C. Fokas, V. Deckert, R. Zenobi, B. Sick, B. Hecht, and U. P. Wild, *Appl. Phys. Lett.* 75, 160 (1999).
46. U. C. Fischer, J. Koglin, and H. Fuchs, *J. Microsc.* 176 (Part 3), 231 (1994).
47. J. Ferber, U. C. Fischer, N. Hagedorn, and H. Fuchs, *Appl. Phys. A* 69, 581 (1999).
48. R. Zenobi and V. Deckert, *Angew. Chem. Int. Ed.* 39, 1746 (2000).
49. K. Nakajima, R. Micheletto, K. Mitsui, T. Isoshima, M. Hara, T. Wada, H. Sasabe, and W. Knoll, *Appl. Surf. Sci.* 144–145, 520 (1999).
50. J. M. Freyland, R. Eckert, and H. Heinzelmann, *Microelectron. Eng.* 53, 653 (2000).
51. S. M. Metev and V. P. Veiko, "Laser Assisted Micro-technology." Springer-Verlag, New York, 1998.
52. M. B. Lee, M. Kourogi, T. Yatsui, K. Tsutsui, N. Atoda, and M. Ohtsu, *Appl. Opt.* 38, 3566 (1999).
53. K. Goto, *J. Appl. Phys.* 37, 2274 (1998).
54. S. Jinang, J. Ichihashi, H. Monobe, M. Fujihira, and M. Ohtsu, *Opt. Commun.* 106, 173 (1994).
55. H. Ueki, Y. Kawata, and S. Kawata, *Appl. Opt.* 35, 2457 (1996).
56. E. B. Cooper, S. R. Manalis, H. Fang, H. Dai, K. Matsumoto, S. C. Minne, T. Hunt, and C. F. Quate, *Appl. Phys. Lett.* 75, 3566 (1999).
57. P. N. Minh, T. Ono, S. Tanaka, K. Goton, and M. Esashi, *Sens. Actuators, A* 95, 168 (2002).
58. C. E. Talley, G. A. Cooksey, and R. C. Dunn, *Appl. Phys. Lett.* 69, 3809 (1996).
59. I. I. Smolyaninov, D. L. Mazzoni, and C. C. Davis, *Appl. Phys. Lett.* 67, 3859 (1995).
60. G. Eggers, A. Rosenberger, N. Held, A. Münnemann, G. Güntherodt, and P. Fumagalli, *Ultramicroscopy* 71, 249 (1998).
61. E. Betzig, J. K. Trautman, R. Wolfe, E. M. Gyorgy, P. L. Finn, M. H. Kryder, and C.-H. Chang, *Appl. Phys. Lett.* 61, 142 (1992).
62. E. S. Snow and P. M. Cambell, *Science* 1639 (1995).
63. M. F. Crommie, C. P. Lutz, and D. M. Eigler, *Science* 262 (1993).
64. V. Foglietti, E. Cianci, and G. Giannini, *Microelectron. Eng.* 57–58, 807 (2001).
65. W. Tan, Z.-Y. Shi, S. Smith, and R. Kopelman, *Mol. Cryst. Liq. Cryst. Sci. Technol., Sect., A* 252, 535 (1994).
66. K. Albert, N. S. Lewis, C. L. Schauer, G. A. Sotzing, S. E. Stitzel, T. P. Vaid, and D. R. Walt, *Chem. Rev.* 100, 2595 (2000).
67. W. R. Seitz, *CRC Crit. Rev. Anal. Chem.* 19, 135 (1988).
68. D. Uttamchandani and S. McCulloch, *Adv. Drug Delivery Rev.* 21, 239 (1996).
69. S. Nie and D. T. Chiu, *Science* 266, 1018 (1994).
70. D. e. a. Zeisel, *Chem. Phys. Lett.* 283, 381 (1998).
71. W. Tan, Z.-Y. Shi, S. Smith, D. Birnbaum, and R. Kopelman, *Science* 258, 778 (1992).
72. B. M. Cullum and T. Vo-Dinh, *Thin Solid Films* 19, 388 (2000).
73. I. Koronczi, J. Reichert, H.-J. Ache, C. Krause, T. Werner, and O. S. Wolfbeis, *Sens. Actuators, B* 74, 47 (2001).
74. D. W. Lubbers, *Sens. Actuators, B* 51, 5 (1998).
75. S. L. Barker, R. Kopelman, T. E. Meyer, and M. A. Cusanovich, *Anal. Chem* 70, 971 (1998).
76. T. Vo-Dinh, J. P. Alarie, and B. M. Cullum, *Fresenius J. Anal. Chem.* 366, 540-551 (2000).
77. T. Vo-Dinh, J. P. Alarie, B. M. Cullum, and G. D. Griffin, *Nat. Biotechnol.* 18, 764 (2000).
78. T. Vo-Dinh, B. M. Cullum, and D. L. Stokes, *Sens. Actuators, B* 74, 2 (2001).
79. S. Arbault, P. Pantano, J. A. Jankowski, M. Vuillaume, and C. Amatore, *Anal. Chem.* 67, 3382 (1995).
80. C. Amatore, S. Arbault, D. Bruce, P. De Oliveira, M. Erard, and M. Vuillaume, *Port. Electrochim. Acta* 19, 145 (2001).
81. C. Amatore, S. Arbault, D. Bruce, P. De Oliveira, M. Erard, and M. Vuillaume, *Chem.—Eur. J.* 7, 4171 (2001).
82. M. T. Kawagoe, J. A. Jankowski, and R. M. Wightman, *Anal. Chem.* 63, 1589 (1991).
83. Y. Nakayama, S. Okazaki, N. Saitou, and H. Wakabayashi, *J. Vac. Sci. Technol., B* 8, 1836 (1990).
84. H. I. Smith, M. L. Schattenburg, S. D. Hector, J. Ferrera, E. E. Moon, I. Y. Yang, and M. Burkhardt, *Microelectron. J.* 32, 143 (1996).
85. L. L. Sohn and R. L. Willett, *Appl. Phys. Lett.* 67, 1552 (1995).
86. Y. Wada, *Microelectron. J.* 29, 601 (1998).
87. S. Sun and G. J. Leggett, *NanoLetters* 2, 1223 (2002).
88. T. H. Dam and P. Pantano, *Rev. Sci. Instrum.* 70, 3982 (1999).
89. Y. Xia, E. Kim, and G. M. Whitesides, *J. Electrochem. Soc.* 143, 1070 (1996).
90. S. Y. Chou, P. R. Krauss, and P. J. Renstrom, *Science* 272, 85 (1996).
91. Y. X. X.-M. Zhao and G. M. Whitesides, *J. Mater. Chem.* 7, 1069 (1997).
92. D. H. Pearson and R. J. Tonucci, *Science* 270, 68 (1995).
93. P. Lambelet, A. Sayah, M. Pfeffer, C. Philipona, and F. Marquis-Weible, *Appl. Opt.* 37, 7289 (1998).
94. T. Held, S. Emonin, O. Martin, and O. Hollricher, *Rev. Sci. Instrum.* 71, 3118 (2000).
95. B. A. F. Puygranier, S. Montgomery, J. Ashe, R. J. Turner, and P. Dawson, *Ultramicroscopy* 86, 233 (2001).
96. G. Krausch, S. Wegscheider, A. Kirsch, and J. Mlynek, *Thin Solid Films* 264, 264 (1995).